Charge-Density-Wave Transitions of Dirac Fermions Coupled to Phonons

Chuang Chen,[1,2] Xiao Yan Xu,[3] Zi Yang Meng,[1,4,5] and Martin Hohenadler[6]

[1]*Beijing National Laboratory for Condensed Matter Physics and Institute of Physics,*
Chinese Academy of Sciences, Beijing 100190, China
[2]*School of Physical Sciences, University of Chinese Academy of Sciences, Beijing 100190, China*
[3]*Department of Physics, Hong Kong University of Science and Technology, Clear Water Bay, Hong Kong, China*
[4]*CAS Center of Excellence in Topological Quantum Computation and School of Physical Sciences,*
University of Chinese Academy of Sciences, Beijing 100190, China
[5]*Songshan Lake Materials Laboratory, Dongguan, Guangdong 523808, China*
[6]*Institut für Theoretische Physik und Astrophysik, Universität Würzburg, 97074 Würzburg, Germany*

The spontaneous generation of charge-density-wave order in a Dirac fermion system via the natural mechanism of electron-phonon coupling is studied in the framework of the Holstein model on the honeycomb lattice. Using two independent and unbiased quantum Monte Carlo methods, the phase diagram as a function of temperature and coupling strength is determined. It features a quantum critical point as well as a line of thermal critical points. Finite-size scaling appears consistent with fermionic Gross-Neveu-Ising universality for the quantum phase transition and bosonic Ising universality for the thermal phase transition. The critical temperature has a maximum at intermediate couplings. Our findings motivate experimental efforts to identify or engineer Dirac systems with sufficiently strong and tunable electron-phonon coupling.

The experimental advances in preparing single-layer graphene [1] have put Dirac fermions at the focus of condensed matter physics. While the single-electron properties are relatively well understood, correlation effects remain a highly active area of research [2]. Because of the two-dimensional (2D) nature of the problem, theoretical models can be analyzed by powerful theoretical and numerical methods, offering the prospect of a comprehensive understanding. The field has recently received another boost by the remarkable properties of other honeycomb systems, in particular, quantum-spin-Hall physics in bismuthene [3] and unconventional superconductivity in twisted bilayer graphene [4]. Finally, massive Dirac phases such as charge-density-wave (CDW) insulators in transition-metal dichalcogenides [5] promise future applications in optoelectronics.

Theoretical studies of massive Dirac fermions in $2 + 1$ dimensions were pioneered by Semenoff [6], who considered a staggered fermion density or CDW, and Haldane [7], who introduced a topological mass that produces an integer quantum Hall state in the absence of a magnetic field. Such problems become even richer if the masses arise from spontaneous symmetry breaking at interaction-driven phase transitions. Particularly remarkable aspects of Dirac systems are that (i) phase transitions occur at nonzero critical values and (ii) the gapless fermionic excitations can strongly modify the critical behavior, giving rise to fermionic quantum critical points [8–17]. The interplay of

different order parameters provides a route to deconfined quantum critical points [18] and emergent symmetries [19,20] (see Ref. [21] for a review).

Numerous interactions have been explored numerically in the framework of honeycomb lattice models. A sufficiently strong on site Hubbard repulsion yields an antiferromagnetic Mott insulator [22–24]. The same holds for a more realistic $1/r$ Coulomb repulsion, although the nonlocal part of the interaction—relevant for graphene where screening is absent—enhances CDW fluctuations [25]. A dominant nearest-neighbor repulsion favors a CDW state [26–30] but is rather unrealistic; for spinful fermions, quantum Monte Carlo (QMC) simulations are hampered by the sign problem. Mean-field predictions of interaction-generated topological states in extended Hubbard models [26] inspired significant efforts to address fluctuation effects. For spinless fermions, unbiased numerical methods reveal the absence of topological phases but support CDW, valence bond solid, and charge-modulated ground states (see Ref. [31] for a review). Similar conclusions were recently reached for the spinful problem [32,33]. Finally, bond-bond interactions were found to produce valence bond, antiferromagnetic, quantum-spin-Hall, and CDW states [12,14,34].

Here, we consider electron-phonon coupling as the mechanism for CDW order. QMC investigations along these lines have so far been restricted by the challenges in simulating electron-phonon models, as addressed by

several recent methodological advances [35–38]. We carried out large-scale QMC simulations of the fundamental Holstein molecular-crystal model [39] to determine the phase diagram as a function of coupling strength and temperature. Moreover, we investigate the nature of the observed quantum and thermal phase transitions.

Model.—Within the Holstein model, electrons coupled to quantum phonons on the honeycomb lattice are described by the Hamiltonian

$$\hat{H} = -t\sum_{\langle ij\rangle\sigma}\hat{c}^{\dagger}_{i\sigma}\hat{c}_{j\sigma} + \sum_{i}\left(\frac{1}{2M}\hat{P}^2_i + \frac{\kappa}{2}\hat{Q}^2_i\right) - g\sum_{i}\hat{Q}_i\hat{\rho}_i. \quad (1)$$

The first term represents nearest-neighbor electronic hopping, the second term describes independent Einstein phonons at each lattice site, and the third term is a coupling between fluctuations of the local electron number $\hat{\rho}_i = \hat{n}_i - 1$ and the lattice displacement $\hat{Q}_i$. Here, $\hat{n}_i = \sum_\sigma \hat{c}^{\dagger}_{i\sigma}\hat{c}_{i\sigma}$, the phonon frequency $\omega_0 = \sqrt{\kappa/M}$, and we introduce the dimensionless coupling $\lambda = g^2/(\kappa W)$ with the free bandwidth $W = 6t$. We consider half-filling and work in units where k_B, $\hbar$, and the lattice constant are equal to 1.

For $\lambda = 0$, Eq. (1) gives the well-known semimetallic band structure $\epsilon(\boldsymbol{k})$ with linear excitations at the Dirac points K, K' [1]. An expansion around these points yields a Dirac equation in terms of eight-component spinor fields corresponding to $N = 2$ (spin $\uparrow, \downarrow$) Dirac fermions with two flavors (valleys K, K') and two pseudospin directions (sublattices A, B) [1].

Methods.—We used the determinant QMC (DQMC) [40] and the continuous-time interaction expansion (CT-INT) QMC methods [41]. In the former, the electrons are integrated out and the phonons are sampled using local and block updates [42,43], as well as global moves based on an effective bosonic model determined by a self-learning scheme [36,44–47] (see Supplemental Material [48]). In CT-INT, the phonons are integrated out and the resulting electronic model with a retarded interaction is sampled [59]. While CT-INT works in continuous imaginary time, a Trotter discretization $\Delta\tau = 0.1$ was used for DQMC calculations. Although both methods are, in principle, capable of simulating any parameters, CT-INT is most efficient at weak coupling and less problematic with respect to autocorrelations [35]. The DQMC method requires more care regarding the sampling but—especially in combination with self-learning—can access stronger couplings and larger system sizes. We used lattices with $L \times L$ unit cells ($2L^2$ sites) and $L = 3n$ ($n = 1, 2, \ldots$) whose reciprocal lattice contains the Dirac points that determine the low-energy physics.

Phase diagram.—The existence of CDW order at sufficiently strong coupling can be inferred from two opposite limits. For classical phonons ($\omega_0 = 0$), we can make a
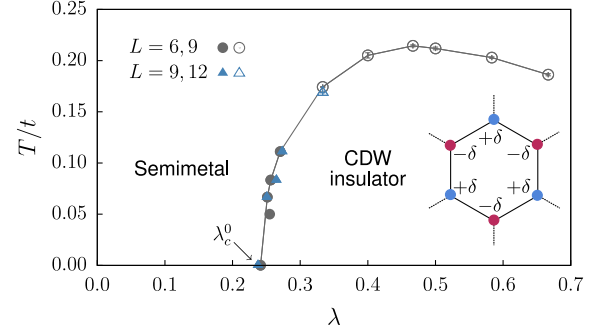

FIG. 1. Phase diagram of the Holstein model (1) for $\omega_0 = 0.5t$. CDW order with a staggered charge disproportionation $\pm\delta$ (inset) exists beyond a quantum critical point at $\lambda^0_c \approx 0.2375$ and below a critical temperature $T_c(\lambda)$. Critical values were obtained from the crossings of the correlation ratio R_c for different system sizes L as a function of λ (filled symbols) or T (open symbols), respectively. Data obtained from CT-INT ($T \leq 0.05t$) and DQMC ($T > 0.05t$) simulations, respectively. The line is a guide to the eye.

mean-field ansatz $\hat{Q}_i \mapsto (-1)^i\bar{Q}$, corresponding to a staggered chemical potential or Semenoff mass that breaks the sublattice and chiral symmetry [6]. The lattice displacements are accompanied by a density imbalance $\delta = |\langle\hat{n}^A\rangle - \langle\hat{n}^B\rangle|$ (see inset of Fig. 1). The band structure acquires a gap at the Fermi level, $E(\boldsymbol{k}) = \pm\sqrt{\epsilon^2(\boldsymbol{k}) + \Delta^2}$. Spontaneous mass generation is described by a gap equation identical to that for the Mott transition of the Hubbard model upon identifying $\bar{Q} = m/2$ ($\Delta = g\bar{Q}$), $\lambda W = U$. The mean-field critical value is $U_c = 2.23t$ or $\lambda_c = 0.37$ [22], which may be compared to $U_c \approx 3.8t$ or $\lambda_c \approx 0.63$ from QMC simulations [23,24,60]. The nonzero critical value reflects the stability of the semimetal at weak coupling [8], the origin of which is the linearly vanishing density of states, $N(\omega) \sim |\omega|$ [1].

In the opposite, antiadiabatic limit $\omega_0 \to \infty$, integrating out the phonons in the path-integral representation yields an attractive Hubbard model with $U = \lambda W$ [61]. By symmetry [62], U_c has the same magnitude as for the Mott transition of the repulsive Hubbard model, namely, $3.8t$ [23,24,60]. Under the Lieb-Mattis particle-hole transformation that yields $U \to -U$, the order parameters for CDW and superconductivity of the attractive Hubbard model combine into a 3D vector that maps to the magnetization of the repulsive model [62]. This implies (i) coexistence of CDW order and superconductivity for $U > U_c$ [63] and (ii) long-range order that spontaneously breaks the SO(3) symmetry only at $T = 0$ [64]. An expansion in $1/\omega_0$ in the path-integral representation of the Holstein model produces terms that violate the SO(3) symmetry [61]. A mean-field decoupling with an Ising CDW order parameter—reflecting the two possible choices for the sign of the excess charge δ in Fig. 1—gives again $U_c = 2.23t$ or $\lambda_c = 0.37$. However, while Ising-like CDW order in the square-lattice Holstein
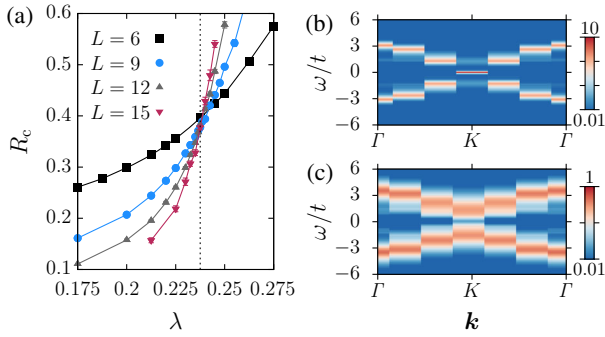
FIG. 2. (a) Estimation of the critical value $\lambda_c^0 \approx 0.2375$ for the quantum critical point from the intersections of the correlation ratio R_c. Here, $\beta t = L$, $\omega_0 = 0.5t$. Single-particle spectral function $A(\boldsymbol{k}, \omega)$ in (b) the semimetallic phase ($\lambda = 0.1$) and (c) the CDW phase ($\lambda = 0.4$) for $\beta t = L = 9$. Results were obtained with the CT-INT method.

model is strongly suggested by the nesting-related, stronger divergence of the CDW susceptibility compared to pairing [65], we are not aware of such an argument for the honeycomb Holstein model considered here.

For quantitative insights into the experimentally relevant case of finite ω_0, we turn to QMC simulations. We focus on $\omega_0 = 0.5t$, for which both quantum fluctuations and retardation effects are significant. We determined critical values either at fixed coupling or at fixed temperature. The values reported in Fig. 1 are based on the renormalization-group (RG)-invariant correlation ratio $R_c = 1 - S_c(\boldsymbol{Q} + \delta\boldsymbol{q})/S_c(\boldsymbol{Q})$ [66] calculated from the charge structure factor $S_c(\boldsymbol{q}) = L^{-2}\sum_{ij}e^{-i\boldsymbol{q}\cdot(\boldsymbol{r}_i - \boldsymbol{r}_j)}\langle(\hat{n}_i^A - \hat{n}_i^B)(\hat{n}_j^A - \hat{n}_j^B)\rangle$. The CDW order is within the unit cell, so the ordering wave vector $\boldsymbol{Q} = \Gamma = (0,0)$. If $\boldsymbol{Q} + \delta\boldsymbol{q}$ is a neighboring point in the Brillouin zone, long-range order and hence a divergence of $S_c(\Gamma)$ implies $R_c \to 1$ for $L \to \infty$, otherwise $R_c \to 0$. At the critical point, R_c is independent of L up to scaling corrections, so that the critical value can be estimated from intersections of R_c for different L. Crucially, the scaling holds independent of any critical exponents and R_c usually has smaller scaling corrections than $S_c(\Gamma)$ [66,67].

Near the quantum critical point, the RG-invariant correlation ratio R_c depends on $(\lambda - \lambda_c)L^{1/\nu}$ and L^z/β. For the finite-size scaling analysis, we took $\beta t = L$ (i.e., $z = 1$) based on the expected emergent Lorentz symmetry [68]. Figure 2(a) suggests a critical value $\lambda_c^0 \approx 0.2375$. Similar analysis for other parameters yields the phase boundary in Fig. 1, shown in terms of the intersections of $L = 6, 9$ and $L = 9, 12$, respectively. Apart from the absence of long-range order at $\lambda < \lambda_c^0$ [Fig. 2(a)], the CDW transition is also apparent in the single-particle spectral function $A(\boldsymbol{k}, \omega)$ (see Supplemental Material [48]). We find gapless excitations at the Dirac point for $\lambda = 0.1$ [Fig. 2(b)] and a gap at the Fermi level for $\lambda = 0.4$ [Fig. 2(c)]. We found no evidence of long-range superconducting order for the parameters considered [48].
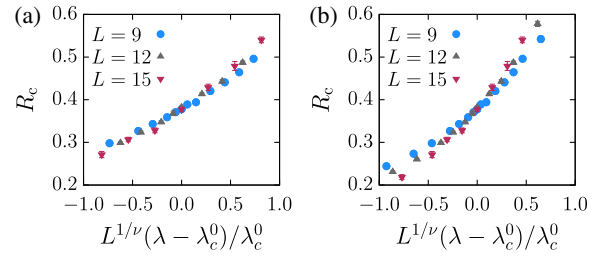

FIG. 3. Scaling collapse of the correlation ratio R_c using $\lambda_c^0 = 0.2375$ and (a) $1/\nu = 1.2$, (b) $1/\nu = 0.931$.

In Fig. 1, CDW order persists up to a critical temperature T_c. After an initial increase, asymptotically determined by the quantum critical point via $T_c \sim |\lambda - \lambda_c^0|^{z\nu}$ [30], T_c takes on a maximum before decreasing at even stronger couplings [69]. This can be understood within an effective t-V model of singlet bipolarons (hardcore bosons) [61]. The binding energy of the latter continues to grow with λ, but their exchange interaction V that sets the temperature for CDW order in this regime decreases (cf. $T_c \sim J$ for the Ising model). An expression for V in the Holstein model is given in Ref. [61] and simplifies to $V \sim t/\lambda$ for $\omega_0 \gg t$. The observed decrease of T_c with increasing electron-phonon coupling λ contrasts the linear increase of T_c with increasing electron-electron repulsion in models for CDW order from Coulomb repulsion [30,70,71]. Finally, the phase boundary is expected to shift to stronger couplings at larger ω_0 due to enhanced lattice fluctuations, reaching $\lambda_c^0 \approx 0.63$ [23,24,60] in the Hubbard limit $\omega_0 \to \infty$, where $T_c \equiv 0$ for any $\lambda > \lambda_c^0$ due to the continuous SO(3) symmetry.

Quantum phase transition.—In Dirac systems, the Yukawa coupling between the gapless fermions and order parameter fluctuations described by Gross-Neveu field theories gives rise to fermionic critical points rather than Wilson-Fisher bosonic critical points [8,9]. Gross-Neveu-Ising universality for CDW transitions was previously observed for $N = 1$ Dirac fermions with nearest-neighbor Coulomb repulsion [27–30] and $N = 2$ Dirac fermions with bond interactions [14,34]. For the Holstein model, Gross-Neveu-*Heisenberg* universality is well established [24,60,72] for $\omega_0 \to \infty$, where it maps to the attractive Hubbard model. The $3 + 1$ dimensional Gross-Neveu theory for the adiabatic limit $\omega_0 \to 0$ should have a correlation length exponent $\nu = 1/2$ [24]. For general ω_0, $2 + 1$ dimensional, $N = 2$ Gross-Neveu-Ising universality is expected.

For a preliminary analysis, we use $\lambda_c^0 = 0.2375$ from Fig. 2(a) and available estimates for the exponent ν from QMC simulations [$1/\nu = 1.2(1)$ [34]] and the ϵ expansion ($1/\nu = 0.931$ [73]), respectively. The rescaled correlation ratio for $L = 9, 12, 15$ in Fig. 3 appears more consistent with $1/\nu = 1.2$ [Fig. 3(a)] than with $1/\nu = 0.931$ [Fig. 3(b)]. As a further consistency check, we determined λ_c^0 from the best scaling collapse [74] on the interval $[-1, 1]$. The exponent $1/\nu = 0.931$ yields $\lambda_c^0 \approx 0.239(2)$, whereas
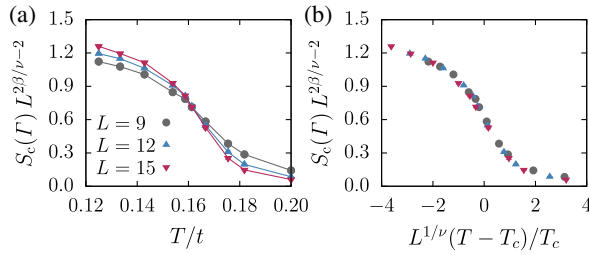
FIG. 4. Finite-size scaling of the density structure factor using the 2D Ising critical exponents $\beta = 1/8$, $\nu = 1$. The critical temperature $T_c = 0.162t$ obtained from the best scaling collapse shown in (b) is consistent with the crossing point in (a). Here, $\omega_0 = 0.5t$, $\lambda = 1/3$. Results obtained with the self-learning DQMC method.

$1/\nu = 1.2$ yields $\lambda_c^0 \approx 0.238(1)$, slightly closer to the value obtained in Fig. 2(a) without any assumption about the value of ν.

A direct estimate of ν based on an improved dataset appears feasible and is motivated by the rather different existing results [73]. At the same time, a potential additional complication—absent in purely fermionic models—is that the phonon frequency interpolates between three different fixed points, namely, mean-field scaling ($\nu = 1/2$ [24]) at $\omega_0 = 0$, Gross-Neveu-Ising scaling for $\omega_0 > 0$, and Gross-Neveu-Heisenberg scaling for $\omega_0 = \infty$. For $\omega_0 = 0.5t$, the proximity to the adiabatic fixed point may give rise to crossover effects in the exponents. Another interesting possibility that has to be ruled out is the formation of singlet pairs—triggered by the attractive component of the frequency-dependent fermion-fermion interaction—prior to the CDW transition, as in the 1D Holstein model [75]. In the absence of gapless fermion excitations at λ_c, Wilson-Fisher theory suggests $2 + 1 = 3$ dimensional Ising universality. Both the expected $\omega_0 = 0$ value ($1/\nu = 2$ [24]) and the 3D Ising value ($1/\nu \approx 1.59$ [76]) are larger than predicted for the $N = 2$ Gross-Neveu-Ising universality class [73].

Thermal phase transition.—Starting from the CDW ground state at $\lambda > \lambda_c^0$, long-range order is destroyed by thermal fluctuations at T_c. The phase transition is expected to exhibit 2D Ising universality with critical exponents $\beta = 1/8$ and $\nu = 1$. Figure 4(a) shows that, for $\omega_0 = 0.5t$ and $\lambda = 1/3$, the rescaled charge structure factor has a crossing of different system sizes compatible with $T_c = 0.159(2)$ in Fig. 1. The best scaling collapse on the interval $[-2, 2]$ produces $T_c = 0.1648(5)t$ and is shown in Fig. 4(b).

Discussion.—Our investigation of spontaneously generated CDW order from electron-phonon coupling on the honeycomb lattice reveals several differences to previous work. Perhaps most importantly, the Dirac band structure gives rise to a quantum critical point with expected Gross-Neveu-Ising universality at nonzero coupling. In contrast, the Fermi liquid of the square lattice is expected to have a weak-coupling instability due to perfect nesting and a van

Hove singularity [35,65]. The thermal CDW transition appears to have the same Ising universality as for the square lattice [35–37,77]. Such a transition is absent in the antiadiabatic limit, corresponding to the attractive Hubbard model. While the latter is useful to describe superconductivity away from half-filling, it supports long-range CDW order only at $T = 0$ [64]. Models with dominant nearest-neighbor repulsion capture the finite-temperature CDW transition [30,70,71] but not the suppression of T_c at strong coupling. Finally, we showed that, similar to the square lattice, CDW order prevails over superconductivity at half-filling.

Outlook.—There are several interesting future directions. The fermionic quantum criticality requires additional efforts. Superconductivity at nonzero doping and the competition between CDW order and antiferromagnetism in a Holstein-Hubbard model should be investigated. Our Letter may also provide a starting point for more realistic modeling of twisted bilayer graphene [4] or transition-metal dichalcogenides [5]. On the experimental side, a key question is if CDW order from electron-phonon coupling can be realized in one of the many Dirac systems currently being investigated.

Note added in proof.—Recently, we became aware of a closely related study of the same model whose results are fully consistent with ours [79].

[1] A. H. C. Neto, F. Guinea, N. M. R. Peres, K. S. Novoselov, and A. K. Geim, Rev. Mod. Phys. **81**, 109 (2009).

[2] H.-K. Tang, J. Leaw, J. Rodrigues, I. Herbut, P. Sengupta, F. Assaad, and S. Adam, Science **361**, 570 (2018).

[3] F. Reis, G. Li, L. Dudy, M. Bauernfeind, S. Glass, W. Hanke, R. Thomale, J. Schäfer, and R. Claessen, Science **357**, 287 (2017).

[4] Y. Cao, V. Fatemi, S. Fang, K. Watanabe, T. Taniguchi, E. Kaxiras, and P. Jarillo-Herrero, Nature (London) **556**, 43 (2018).

[5] S. Manzeli, D. Ovchinnikov, D. Pasquier, O. V. Yazyev, and A. Kis, Nat. Rev. Mater. **2**, 17033 (2017).

[6] G. W. Semenoff, Phys. Rev. Lett. **53**, 2449 (1984).

[7] F. D. M. Haldane, Phys. Rev. Lett. **61**, 2015 (1988).

[8] I. F. Herbut, Phys. Rev. Lett. **97**, 146401 (2006).

[9] I. F. Herbut, V. Juričić, and O. Vafek, Phys. Rev. B **80**, 075432 (2009).

[10] M. M. Scherer and I. F. Herbut, Phys. Rev. B **94**, 205136 (2016).

[11] Z. Zhou, D. Wang, Z. Y. Meng, Y. Wang, and C. Wu, Phys. Rev. B **93**, 245157 (2016).

[12] Z.-X. Li, Y.-F. Jiang, S.-K. Jian, and H. Yao, Nat. Commun. **8**, 314 (2017).

[13] L. Classen, I. F. Herbut, and M. M. Scherer, Phys. Rev. B **96**, 115132 (2017).

[14] Y.-Y. He, X. Y. Xu, K. Sun, F. F. Assaad, Z. Y. Meng, and Z.-Y. Lu, Phys. Rev. B **97**, 081110 (2018).

[15] E. Torres, L. Classen, I. F. Herbut, and M. M. Scherer, Phys. Rev. B **97**, 125137 (2018).

[16] X. Y. Xu, K. T. Law, and P. A. Lee, Phys. Rev. B **98**, 121406 (2018).

[17] T. C. Lang and A. M. Läuchli, arXiv:1808.01230.

[18] T. Senthil, A. Vishwanath, L. Balents, S. Sachdev, and M. P. A. Fisher, Science **303**, 1490 (2004).

[19] T. Sato, M. Hohenadler, and F. F. Assaad, Phys. Rev. Lett. **119**, 197203 (2017).

[20] Y. Q. Qin, Y.-Y. He, Y.-Z. You, Z.-Y. Lu, A. Sen, A. W. Sandvik, C. Xu, and Z. Y. Meng, Phys. Rev. X **7**, 031052 (2017).

[21] C. Wang, A. Nahum, M. A. Metlitski, C. Xu, and T. Senthil, Phys. Rev. X **7**, 031051 (2017).

[22] S. Sorella and E. Tosatti, Europhys. Lett. **19**, 699 (1992).

[23] S. Sorella, Y. Otsuka, and S. Yunoki, Sci. Rep. **2**, 992 (2012).

[24] F. F. Assaad and I. F. Herbut, Phys. Rev. X **3**, 031010 (2013).

[25] M. Hohenadler, F. Parisen Toldin, I. F. Herbut, and F. F. Assaad, Phys. Rev. B **90**, 085146 (2014).

[26] S. Raghu, X.-L. Qi, C. Honerkamp, and S.-C. Zhang, Phys. Rev. Lett. **100**, 156401 (2008).

[27] E. F. Huffman and S. Chandrasekharan, Phys. Rev. B **89**, 111101 (2014).

[28] L. Wang, P. Corboz, and M. Troyer, New J. Phys. **16**, 103008 (2014).

[29] Z.-X. Li, Y.-F. Jiang, and H. Yao, New J. Phys. **17**, 085003 (2015).

[30] S. Hesselmann and S. Wessel, Phys. Rev. B **93**, 155157 (2016).

[31] S. Capponi, J. Phys. Condens. Matter **29**, 043002 (2017).

[32] D. S. de la Peña, J. Lichtenstein, and C. Honerkamp, Phys. Rev. B **95**, 085143 (2017).

[33] M. Bijelic, R. Kaneko, C. Gros, and R. Valentí, Phys. Rev. B **97**, 125142 (2018).

[34] S. Chandrasekharan and A. Li, Phys. Rev. D **88**, 021701 (2013).

[35] M. Weber and M. Hohenadler, Phys. Rev. B **98**, 085405 (2018).

[36] C. Chen, X. Y. Xu, J. Liu, G. Batrouni, R. Scalettar, and Z. Y. Meng, Phys. Rev. B **98**, 041102 (2018).

[37] G. G. Batrouni and R. T. Scalettar, Phys. Rev. B **99**, 035114 (2019).

[38] S. Karakuzu, K. Seki, and S. Sorella, Phys. Rev. B **98**, 201108 (2018).

[39] T. Holstein, Ann. Phys. (N.Y.) **8**, 325 (1959); **8**, 343 (1959).

[40] R. Blankenbecler, D. J. Scalapino, and R. L. Sugar, Phys. Rev. D **24**, 2278 (1981).

[41] A. N. Rubtsov, V. V. Savkin, and A. I. Lichtenstein, Phys. Rev. B **72**, 035122 (2005).

[42] R. T. Scalettar, R. M. Noack, and R. R. P. Singh, Phys. Rev. B **44**, 10502 (1991).

[43] S. Johnston, E. A. Nowadnick, Y. F. Kung, B. Moritz, R. T. Scalettar, and T. P. Devereaux, Phys. Rev. B **87**, 235133 (2013).

[44] J. Liu, Y. Qi, Z. Y. Meng, and L. Fu, Phys. Rev. B **95**, 041101 (2017).

[45] J. Liu, H. Shen, Y. Qi, Z. Y. Meng, and L. Fu, Phys. Rev. B **95**, 241104 (2017).

[46] X. Y. Xu, Y. Qi, J. Liu, L. Fu, and Z. Y. Meng, Phys. Rev. B **96**, 041119 (2017).

[47] Y. Nagai, H. Shen, Y. Qi, J. Liu, and L. Fu, Phys. Rev. B **96**, 161102 (2017).

[48] See Supplemental Material at http://link.aps.org/supplemental/10.1103/PhysRevLett.122.077601, which includes Refs. [36,44–47,49–58], for methodological details and additional data.

[49] L. Huang and L. Wang, Phys. Rev. B **95**, 035105 (2017).

[50] L. Huang, Y. F. Yang, and L. Wang, Phys. Rev. E **95**, 031301 (2017).

[51] Z. H. Liu, X. Y. Xu, Y. Qi, K. Sun, and Z. Y. Meng, Phys. Rev. B **98**, 045116 (2018).

[52] Z. H. Liu, X. Y. Xu, Y. Qi, K. Sun, and Z. Y. Meng, arXiv:1801.00127.

[53] Z. H. Liu, G. Pan, X. Y. Xu, K. Sun, and Z. Y. Meng, arXiv:1808.08878.

[54] R. H. Swendsen and J.-S. Wang, Phys. Rev. Lett. **58**, 86 (1987).

[55] U. Wolff, Phys. Rev. Lett. **62**, 361 (1989).

[56] S. Duane, A. D. Kennedy, B. J. Pendleton, and D. Roweth, Phys. Lett. B **195**, 216 (1987).

[57] K. S. D. Beach, arXiv:cond-mat/0403055.

[58] M. Bercx, F. Goth, J. S. Hofmann, and F. F. Assaad, SciPost Phys. **3**, 013 (2017).

[59] F. F. Assaad and T. C. Lang, Phys. Rev. B **76**, 035116 (2007).

[60] F. Parisen Toldin, M. Hohenadler, F. F. Assaad, and I. F. Herbut, Phys. Rev. B **91**, 165108 (2015).

[61] J. E. Hirsch and E. Fradkin, Phys. Rev. B **27**, 4302 (1983).

[62] C. N. Yang and S. Zhang, Mod. Phys. Lett. B **04**, 759 (1990).

[63] E. Zhao and A. Paramekanti, Phys. Rev. Lett. **97**, 230404 (2006).

[64] J. E. Hirsch, Phys. Rev. B **31**, 4403 (1985).

[65] F. Marsiglio, Phys. Rev. B **42**, 2416 (1990).

[66] K. Binder, Z. Phys. B Condens. Matter **43**, 119 (1981).

[67] S. Pujari, T. C. Lang, G. Murthy, and R. K. Kaul, Phys. Rev. Lett. **117**, 086404 (2016).

[68] I. F. Herbut, V. Juričić, and B. Roy, Phys. Rev. B **79,** 085116 (2009).

[69] S. Blawid and A. J. Millis, Phys. Rev. B **63,** 115114 (2001).

[70] J. E. Gubernatis, D. J. Scalapino, R. L. Sugar, and W. D. Toussaint, Phys. Rev. B **32,** 103 (1985).

[71] M. Bercx, J. S. Hofmann, F. F. Assaad, and T. C. Lang, Phys. Rev. B **95,** 035108 (2017).

[72] Y. Otsuka, S. Yunoki, and S. Sorella, Phys. Rev. X **6,** 011029 (2016).

[73] N. Zerf, L. N. Mihaila, P. Marquard, I. F. Herbut, and M. M. Scherer, Phys. Rev. D **96,** 096010 (2017).

[74] O. Melchert, arXiv:0910.5403.

[75] M. Hohenadler and F. F. Assaad, Phys. Rev. B **87,** 075149 (2013).

[76] M. Hasenbusch, K. Pinn, and S. Vinti, Phys. Rev. B **59,** 11471 (1999).

[77] N. C. Costa, T. Blommel, W.-T. Chiu, G. Batrouni, and R. T. Scalettar, Phys. Rev. Lett. **120,** 187003 (2018).

[78] Jülich Supercomputing Centre, J. Large-Scale Res. Facilities **2,** A62 (2016).

[79] Y.-X. Zhang, W.-T. Chiu, N. C. Costa, G. G. Batrouni, and R. T. Scalettar, following Letter, Phys. Rev. Lett. **122,** 077602 (2019).